Anion−π Interaction Guided Switchable TADF and Low-Temperature Phosphorescence in Phosphonium Salts for Multiplexed Anti-Counterfeiting

Jun-Hua Wei[1], Yao Xiao[1], Jian-Bin Luo[1], Zi-Lin He[1], Jing-Hua Chen[1], Qing-Peng Peng[1], and Dai-Bin Kuang[1]*

[1]Key Laboratory of Bioinorganic and Synthetic Chemistry of Ministry of Education, LIFM, GBRCE for Functional Molecular Engineering, School of Chemistry, IGCME, Sun Yat-Sen University, Guangzhou, 510275 China.

Corresponding author

*Email: D.-B.K. (kuangdb@mail.sysu.edu.cn).

Contents

Materials and preparation

2-diphenylphosphino-2'-(N,N-dimethylamino)biphenyl (Bidepharm, 98%), toluene (Guangzhou Chemical Reagent, A.R.), 1-iodopropane (Aladdin, >98.0%), ethyl acetate (EA, Greagent, ≥99.5%), dichloromethane (CH_2Cl_2, Guangzhou Chemical Reagent, A.R.), methanol (MeOH, Guangzhou Chemical Reagent, A.R.), ethanol (EtOH, Guangzhou Chemical Reagent, A.R.), n-propanol (n-PA, Aladdin, 99.5%), n-butanol (BuOH, Guangzhou Chemical Reagent, A.R.), acetone (AC, Guangzhou Chemical Reagent, A.R.), acetonitrile (ACN, Aladdin, >99.8%), propylene carbonate (PC, Aladdin, ≥98%), N,N-dimethylformamide (DMF, Aladdin, >99.9%), dimethyl sulfoxide (DMSO, Aladdin, >99%), silver tetrafluoroborate ($AgBF_4$, Aladdin, 99%), silver perchlorate ($AgClO_4$, Macklin, 97%), silver nitrate ($AgNO_3$, Aladdin, 99.8%), silver trifluoromethanesulfonate ($AgCF_3SO_3$, Bidepharm, 98%), two-part PDMS DC184 encapsulant (Dow-Corning). All reagents were used as received without further purification.

2-diphenylphosphino-2'-(N,N-dimethylamino)biphenyl: 1H NMR (400 MHz, DMSO-d6) δ 7.48 (dd, *J* = 8.0, 6.7 Hz, 1H), 7.42 – 7.32 (m, 5H), 7.32 – 7.26 (m, 4H), 7.21 – 7.12 (m, 3H), 7.06 – 7.00 (m, 3H), 6.92 (d, *J* = 4.4 Hz, 2H), 2.20 (s, 6H). ^{31}P NMR (162 MHz, DMSO-d6) δ -14.78.

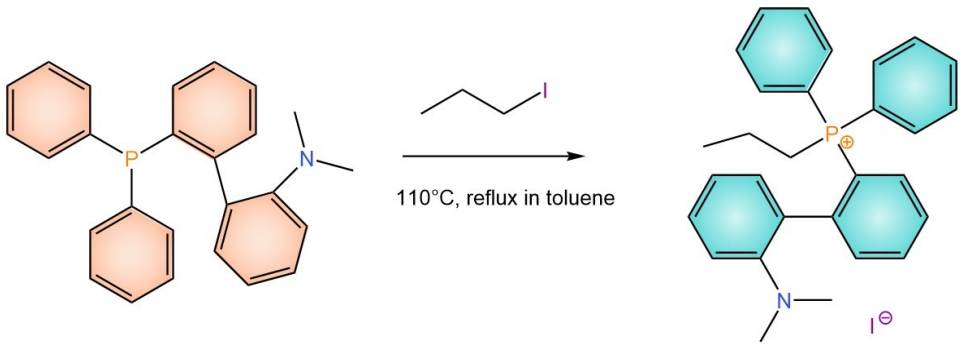

Scheme S1. Preparation procedure of phosphonium iodides.

The synthesis route of the propyl(2-[2-(dimethylamino)phenyl]phenyl)diphenylphosphonium iodide powders

In a round-bottom flask, 2-diphenylphosphino-2'-(N,N-dimethylamino)biphenyl and 1-iodopropane at a molar ratio of 1:1.25 were dissolved in toluene to form a clear solution, where 1 mmol 2-diphenylphosphino-2'-(N,N-dimethylamino)biphenyl consumes 10 mL toluene. The mixture was stirred at 110°C for 24 h to obtain the white powders, which were collected through filtration and then washed with ethyl acetate. The obtained powders were dried to remove the excess solvent.

^{1}H NMR (400 MHz, DMSO-d6) δ 8.05 – 7.96 (m, 1H), 7.88 – 7.70 (m, 8H), 7.70 – 7.64 (m, 1H), 7.61 (td, *J* = 7.8, 3.3 Hz, 2H), 7.42 – 7.30 (m, 3H), 7.20 (dd, *J* = 7.5, 1.7 Hz, 1H), 7.04 (td, *J* = 7.4, 1.0 Hz, 1H), 6.85 (d, *J* = 8.1 Hz, 1H), 2.84 (ddd, *J* = 25.0, 14.2, 4.9 Hz, 1H), 2.28 – 2.15 (m, 1H), 1.83 (s, 6H), 1.24 (s, 2H), 0.67 (td, *J* = 7.2, 2.1 Hz, 3H).

^{31}P NMR (162 MHz, DMSO-d6) δ 25.39.

Preparation of C3-I single crystals

Similar to the preparation of C3-I powders, 2-diphenylphosphino-2'-(N,N-dimethylamino)biphenyl and 1-iodopropane at a molar ratio of 1:1.25 were employed as the raw materials, which were then dissolved in toluene at room temperature for form a clear precursor solution. The solution was sealed by a parafilm and stored at room temperature. Transparent single crystals were precipitated from the solution after being stored for 48 h. The obtained single crystals were used to determine the crystal structure.

Preparation of C3-I powders containing dichloromethane molecules

The blue-emitting C3-I powders were dissolved in dichloromethane, and then ethyl acetate was added as the anti-solvent. The mixed solution was placed in a fume cupboard. Needle-like polycrystals were precipitated as the evaporation of the solvent.

Preparation of C3-X through ion exchanging with Ag(I)-X

The general synthesis procedure of C3-X involves the direct ion exchange between C3-I and Ag(I)-X. Firstly, the C3-I powders were dissolved in dichloromethane, which was then mixed with the solution of Ag(I)-X (e.g., $AgBF_4$, $AgClO_4$, $AgNO_3$, $AgCF_3SO_3$) in acetone. The mixed solution was stirred for 3 h under dark conditions to avoid the decomposition of AgI sediment, and then the precipitated AgI was discarded. Ethyl acetate was added to the resulting solution, which was stored to evaporate the solvent. C3-X single crystals were precipitated and collected through filtration.

C3-BF_4

^{1}H NMR (400 MHz, DMSO-d6) δ 8.05 – 7.96 (m, 1H), 7.88 – 7.69 (m, 8H), 7.69 – 7.54 (m, 3H), 7.36 (m, 3H), 7.22 – 7.15 (m, 1H), 7.07 – 6.98 (m, 1H), 6.88 – 6.80 (m, 1H), 2.88 – 2.71 (m, 1H), 2.21 (q, *J* = 14.0 Hz, 1H), 1.89 – 1.75 (m, 6H), 1.22 (br, 2H), 0.73 – 0.60 (m, 3H).

^{31}P NMR (162 MHz, DMSO) δ 25.3.

^{19}F NMR (377 MHz, DMSO-d6) δ -148.20 – -148.30 (m).

C3-ClO_4

^{1}H NMR (400 MHz, DMSO-d6) δ 8.06 – 7.96 (m, 1H), 7.88 – 7.69 (m, 8H), 7.69 – 7.55 (m, 3H), 7.34 (m, 3H), 7.19 (dd, *J* = 7.5, 1.8 Hz, 1H), 7.03 (t, *J* = 7.5 Hz, 1H), 6.85 (d, *J* = 8.2 Hz, 1H), 2.90 – 2.73 (m, 1H), 2.22 (q, *J* = 13.6, 11.9 Hz, 1H), 1.84 (s, 6H), 1.24 – 1.12 (m, 2H), 0.72 – 0.61 (m, 3H).

^{31}P NMR (162 MHz, DMSO) δ 25.3.

C3-PF_6

^{1}H NMR (400 MHz, DMSO-d6) δ 8.02 (t, *J* = 7.4 Hz, 1H), 7.88 – 7.71 (m, 8H), 7.69 – 7.58 (m, 3H), 7.36 (m, 3H), 7.20 (d, *J* = 7.5 Hz, 1H), 7.03 (t, *J* = 7.4 Hz, 1H), 6.85 (d, *J* = 8.2 Hz, 1H), 2.84 (q, *J* = 16.9, 13.7 Hz, 1H), 2.23 (q, *J* = 13.6 Hz, 1H), 1.84 (s, 6H), 1.20 (d, *J* = 17.8 Hz, 2H), 0.68 (t, *J* = 7.3 Hz, 3H).

^{31}P NMR (162 MHz, DMSO) δ 25.4, -135.4, -139.8, -144.2, -148.6, -153.0.

^{19}F NMR (377 MHz, DMSO-d6) δ -70.16 (d, *J* = 711.4 Hz).

C3-CF_3SO_3

^{1}H NMR (400 MHz, DMSO-d6) δ 8.01 (d, *J* = 7.5 Hz, 1H), 7.88 – 7.71 (m, 8H), 7.70 – 7.57 (m, 3H), 7.36 (m, 3H), 7.20 (d, *J* = 7.5 Hz, 1H), 7.03 (t, *J* = 7.5 Hz, 1H), 6.85 (d,

J = 8.2 Hz, 1H), 2.91 – 2.76 (m, 1H), 2.23 (q, *J* = 14.8, 13.4 Hz, 1H), 1.84 (s, 6H), 1.19 (m, 2H), 0.68 (t, *J* = 7.4 Hz, 3H).

^{31}P NMR (162 MHz, DMSO) δ 25.4.

^{19}F NMR (377 MHz, DMSO-d6) δ -77.74.

C3-NO_3

^{1}H NMR (400 MHz, DMSO-d6) δ 8.01 (d, *J* = 7.5 Hz, 1H), 7.87 – 7.71 (m, 8H), 7.87 – 7.58 (m, 3H), 7.36 (m, 3H), 7.20 (d, *J* = 7.5 Hz, 1H), 7.03 (t, *J* = 7.5 Hz, 1H), 6.85 (d, *J* = 8.2 Hz, 1H), 2.84 (m, 1H), 2.23 (q, *J* = 15.4, 13.4 Hz, 1H), 1.84 (s, 6H), 1.21 (d, *J* = 18.1 Hz, 2H), 0.68 (t, *J* = 7.2 Hz, 3H).

^{31}P NMR (162 MHz, DMSO) δ 25.4.

Preparation of C4-I powders and single crystals

The preparation of C4-I powders is the same as C3-I powders, except that 1-iodopropane was replaced by 1-iodobutane. For the preparation of C4-I single crystals, In detail, C4-I powders were dissolved in dichloromethane, and then ethyl acetate was used as the anti-solvent (V_{DCM} : V_{EA}=1:2). Transparent C4-I single crystals were precipitated from the mixed solutions as the evaporation of the solvent.

NMR analysis results of C4-I single crystals: 1H NMR (400 MHz, DMSO-d6) δ 8.01 (m, 1H), 7.88 – 7.71 (m, 8H), 7.70 – 7.57 (m, 3H), 7.39 (m, 2H), 7.33 (m, 1H), 7.21 (m, 1H), 7.03 (m, 1H), 6.90 – 6.77 (m, 1H), 2.89 – 2.73 (m, 1H), 2.39 – 2.22 (m, 1H), 1.84 (s, 6H), 1.23 – 1.02 (m, 3H), 0.97 (m, 1H), 0.70 (t, *J* = 7.1 Hz, 3H).

Measurements and characterizations

Single-crystal diffraction measurements (SCXRD) of C3-I, C3-BF_4, and C3-CF_3SO_3 were carried out on the Bruker D8 Venture diffractometer at 100 K with Mo Kα (λ = 0.71073 Å) radiation. The samples for the NMR test were dissolved in DMSO-d6. Nuclear magnetic resonance (NMR) spectra were collected on a Bruker Avance NEO 400MHz spectrometer. Powder X-ray diffraction (PXRD) analysis was carried out on Miniflex600 diffractometer (Rigaku) with Cu Kα radiation (λ = 1.54 Å). Steady-state PL spectra and time-resolved PL spectra were performed on a PL spectrometer

(FLS1000, Edinburgh Instruments Ltd.). Temperature-dependent PL spectra were carried out on FLS980 by employing a Xe lamp as the excitation source, and the sample was cooled by liquid nitrogen. PL quantum yields (PLQYs) were recorded on Hamamatsu instruments C9920. Thermogravimetric analysis (TGA) was carried out on TG209F1 libra TGA system with a heating rate of 10 K/min under N_2 atmosphere. Differential scanning calorimetry (DSC) data were collected on Netzsch DSC-204 F1.

Theoretical calculations

The density function theory calculations of C3-I, C3-BF_4, and C3-CF_3SO_3 were performed by using the CP2K[1] package without considering the solvent effect. The periodic calculation of C3-I, C3-BF_4, and C3-CF_3SO_3 was carried out by adopting the PBE0[2] hybrid density function with Grimme D3 correction[3]. The Goedecker-Teter-Hutter (GTH) pseudopotentials[4], DZVP-MOLOPT-SR-GTH basis sets[5] were utilized to describe the molecules. A plane-wave energy cut-off of 600 Ry has been employed. The excited states were investigated by time-dependent DFT calculation[6], and the transitions between the ground state and the lowest ten excited states were considered. The excitation analyses were studied on the multifunctional wavefunction (Multiwfn) analyzer.[7,8] The visualization of molecular orbitals was performed by using the VESTA package.[9]

The calculation of interaction energy was performed by using single-point energy calculation through the B3LYP/def2-TZVP method, and the basis set superposition error (BSSE) was included. The interaction energy is calculated through the following formula, $E_{interaction} = E_{complex} - E_{anion} - E_{cation} + E_{BSSE}$, where $E_{complex}$, E_{anion}, E_{cation}, and E_{BSSE} are the energies of C3-X complex, X^- anion, $C3^+$ cation, and BSSE. The calculations are performed by the Gaussian 16 package[10] based on the experimental single-crystal structures of C3-X.

Table S1. Single-crystal X-ray diffraction data of C3-I, C3-BF_4, and C3-CF_3SO_3 single crystal.

Compound	C3-I	C3-BF_4	C3-CF_3SO_3
Empirical formula	$C_{29}H_{31}INP$	$C_{29}H_{31}BF_4NP$	$C_{30}H_{31}F_3NPSO_3$
Formula weight	551.42	511.33	573.59
Temperature/K	155.0	99.99	100.0
Crystal system	monoclinic	monoclinic	orthorhombic
Space group	$P2_1/c$	$P2_1/n$	P212121
a/Å	11.1724(9)	9.6378(8)	9.2871(3)
b/Å	14.0119(9)	8.2283(8)	13.5822(5)
c/Å	17.0939(12)	32.674(3)	21.8141(8)
α/°	90	90	90
β/°	99.724(4)	94.380(3)	90
γ/°	90	90	90
Volume/$Å^3$	2637.5(3)	2583.6(4)	2751.61(17)
Z	4	4	4
$\rho_{calc}g/cm^3$	1.389	1.315	1.385
μ/mm^{-1}	1.291	0.154	0.229
F(000)	1120.0	1072.0	1200.0
Radiation	MoKα (λ = 0.71073)	MoKα (λ = 0.71073)	MoKα (λ = 0.71073)
2Θ range for data collection/°	3.698 to 51.368	5.002 to 53.084	4.766 to 53.048
Index ranges	$-13 \le h \le 13$, $-17 \le k \le 17$, $-20 \le l \le 20$	$-11 \le h \le 12$, $-10 \le k \le 10$, $-41 \le l \le 40$	$-11 \le h \le 11$, $-17 \le k \le 16$, $-27 \le l \le 27$
Reflections collected	27636	25886	29086
Independent reflections	4976 [R_{int} = 0.0840, R_{sigma} =	5348 [R_{int} = 0.0863, R_{sigma} =	5704 [Rint = 0.0661, Rsigma =

	0.0640]	0.0677]	0.0437]
Data/restraints/parameters	4976/0/292	5348/0/328	5704/0/355
Goodness-of-fit on F^2	1.092	1.046	1.047
Final R indexes [I>=2σ (I)]	R_1 = 0.0545, wR_2 = 0.1395	R_1 = 0.0430, wR_2 = 0.0960	R_1 = 0.0332, wR_2 = 0.0735
Final R indexes [all data]	R_1 = 0.0710, wR_2 = 0.1465	R_1 = 0.0639, wR_2 = 0.1078	R_1 = 0.0387, wR_2 = 0.0772
Largest diff. peak/hole / e $Å^{-3}$	2.44/-0.94	0.27/-0.45	0.26/-0.29

Table S2. The elemental analysis results of C3-I.

	C (%)	**H (%)**	**N (%)**
Theoretical	63.16	5.67	2.54
Experimental 1	63.51	5.84	2.27
Experimental 2	63.37	5.77	2.25

Table S3. The calculated rate constants for C3-I and C3-X.

	$\emptyset_{PL}$	$\emptyset_{PF}$	$\emptyset_{DF}$	k_{ISC}	k_{RISC}
C3-I	0.753	0.016	0.737	1.91×10^{8} s^{-1}	1.78×10^{5} s^{-1}
C3-BF_4	0.798	0.140	0.658	5.40×10^{7} s^{-1}	1.09×10^{4} s^{-1}
C3-CF_3SO_3	0.991	0.393	0.598	1.21×10^{7} s^{-1}	4.26×10^{3} s^{-1}

The rate constants are calculated through equations S1-S6 by assuming that $k_{nr}^{S} \approx 0$, (k_{nr}^{S} is the rate constant of the non-radiative decay of singlet excitons):[1, 2]

$$k_{PF} = \frac{1}{\tau_{PF}} \quad \text{(S1)}$$

$$k_{DF} = \frac{1}{\tau_{DF}} \quad \text{(S2)}$$

$$k_r^S = \emptyset_{PF} k_{PF} \quad \text{(S3)}$$

$$k_{ISC} = k_{PF}(1 - \emptyset_{PF}) \quad \text{(S4)}$$

$$k_{RISC} = \frac{k_{PF} k_{DF} \emptyset_{DF}}{k_{ISC}\ \emptyset_{PF}} \quad \text{(S5)}$$

$$k_{nr}^T = k_{DF} - \emptyset_{PF} k_{RISC} \quad \text{(S6)}$$

where k_{PF} is the prompt fluorescence rate constant, k_{DF} is the delayed fluorescence rate constant, $\emptyset_{PL}$is the measured overall quantum yield, $\emptyset_{PF}$and $\emptyset_{DF}$ are the quantum yields of prompt fluorescence and delayed fluorescence, k_{ISC} and k_{RISC} are the rate constants of ISC and RISC, k_r^S and k_{nr}^S are the radiative and non-radiative decay rate constants for fluorescence (S_1 to S_0), k_{nr}^T is the rate constant of the non-radiative decay of triplet excitons.

Table S4. The PL positions and solvent polarity of C3-I solutions.

	solvent polarity	PL position (nm)
DCM (dichloromethane)	3.4	512
BuOH (n-butanol)	3.9	534
n-PA (n-propanol)	4.0	534
EtOH (ethanol)	4.3	537
MeOH (methanol)	5.1	538
AC (acetone)	5.4	543
ACN (acetonitrile)	5.8	546
PC (propylene carbonate)	6.1	547
DMF (N,N-dimethylformamide)	6.4	553
DMSO (dimethyl sulfoxide)	7.2	556
H_2O (Water)	10.2	561

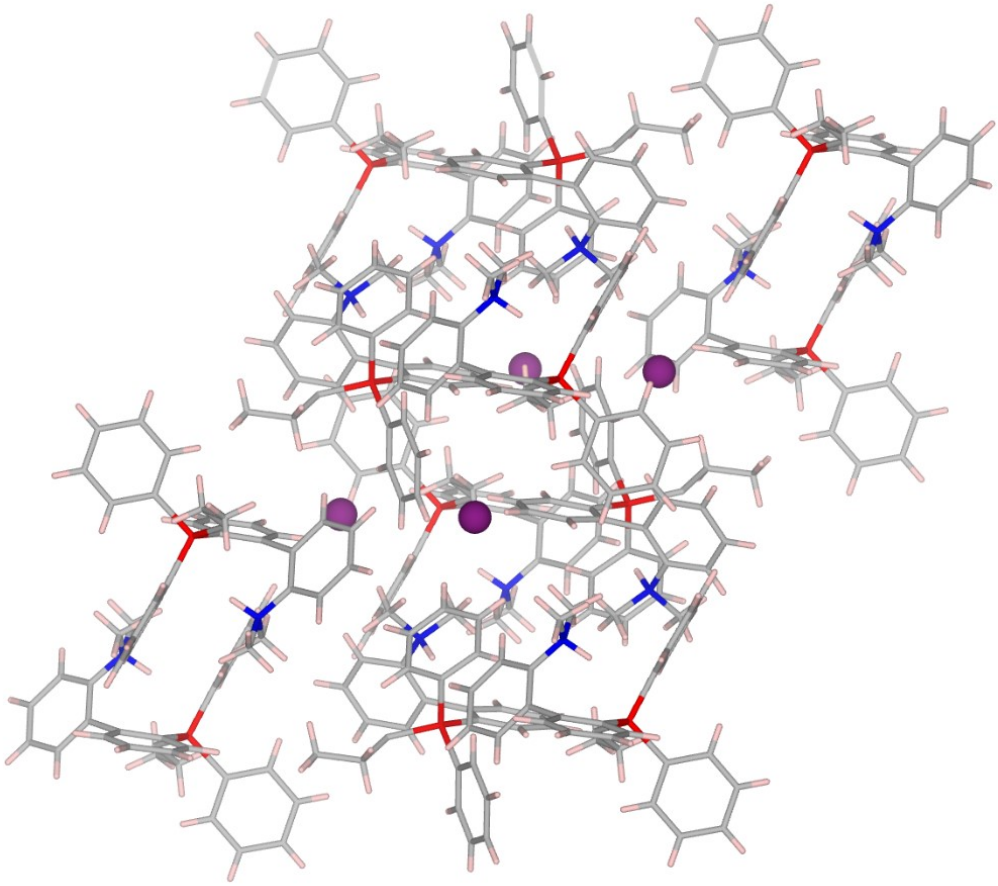

Fig. S1. Crystal structure of C3-I.

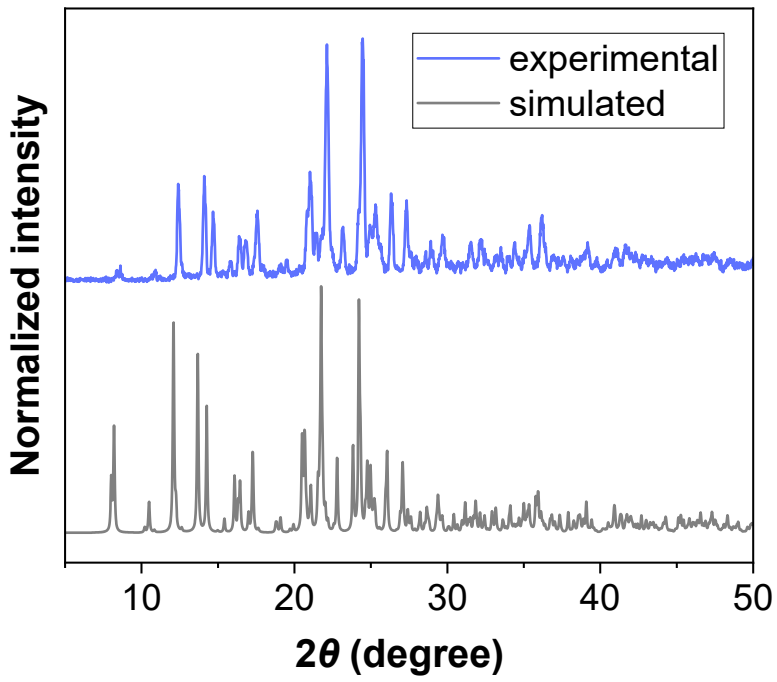

Fig. S2. Comparison of the experimental and simulated PXRD patterns of C3-I.

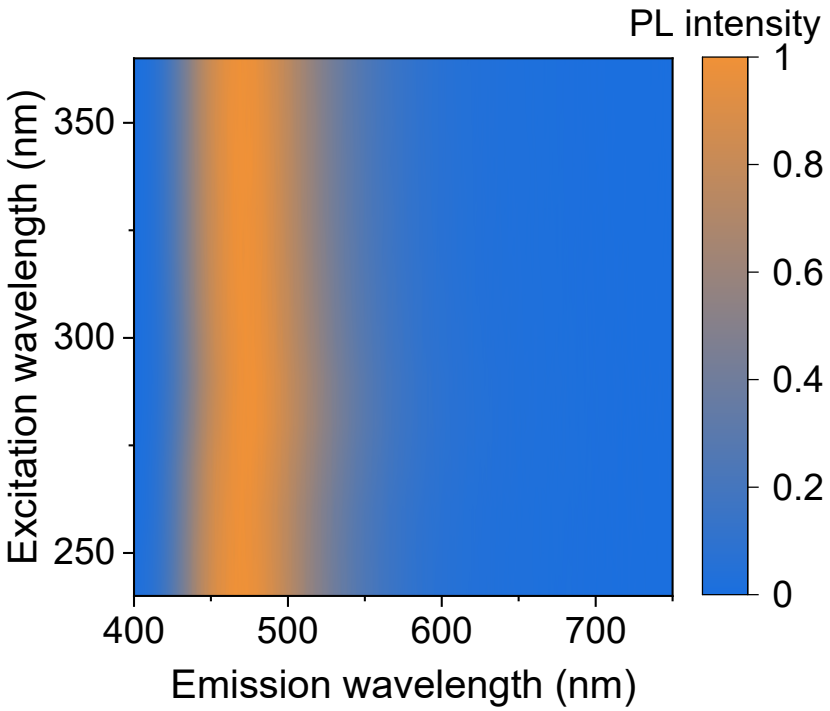

Fig. S3. Excitation-wavelength-dependent PL spectra of C3-I powders.

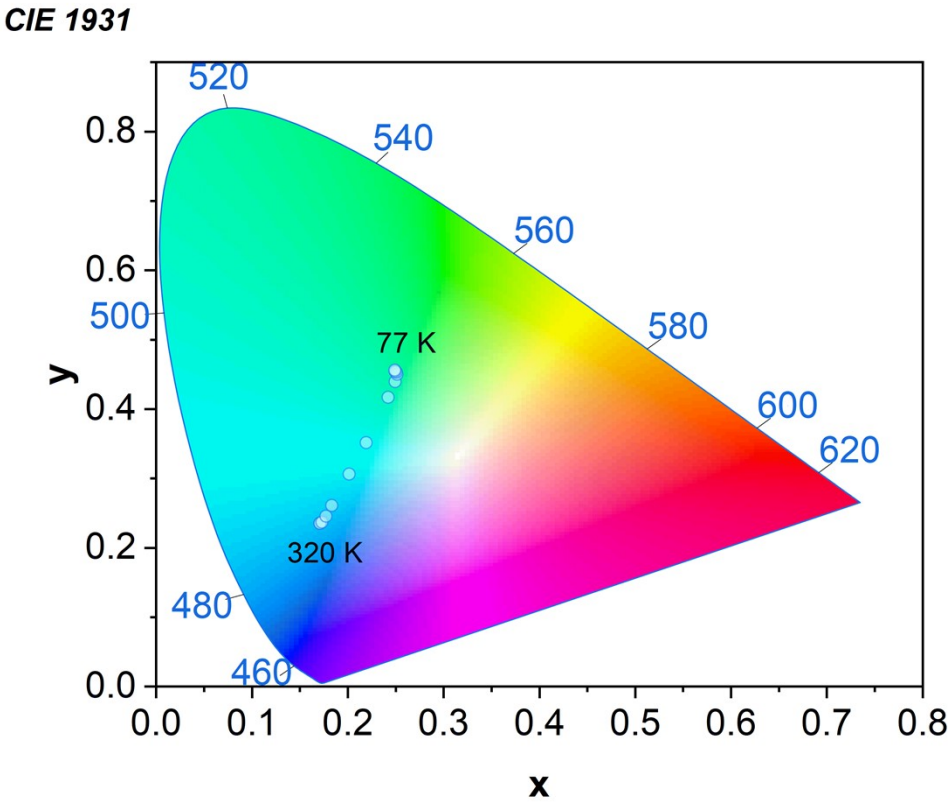

Fig. S4. Temperature-dependent CIE coordinates of C3-I.

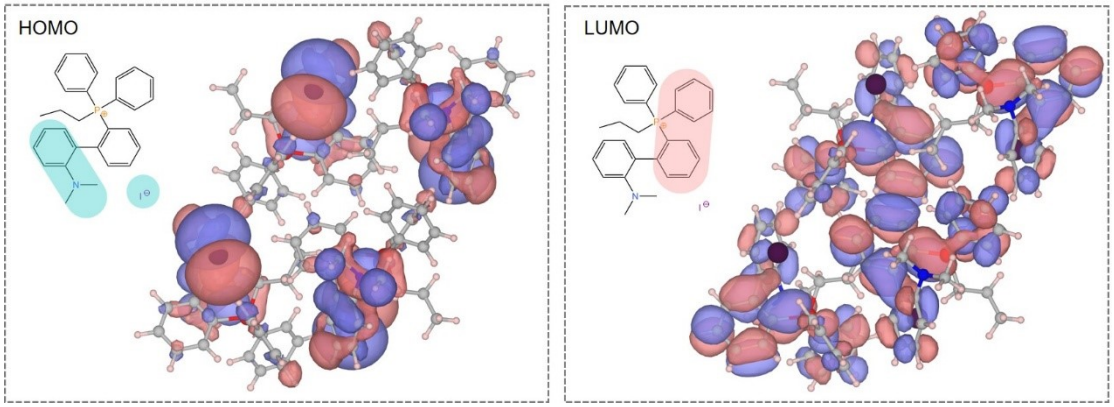

Fig. S5. The electron distributions of HOMO and LUMO orbitals.

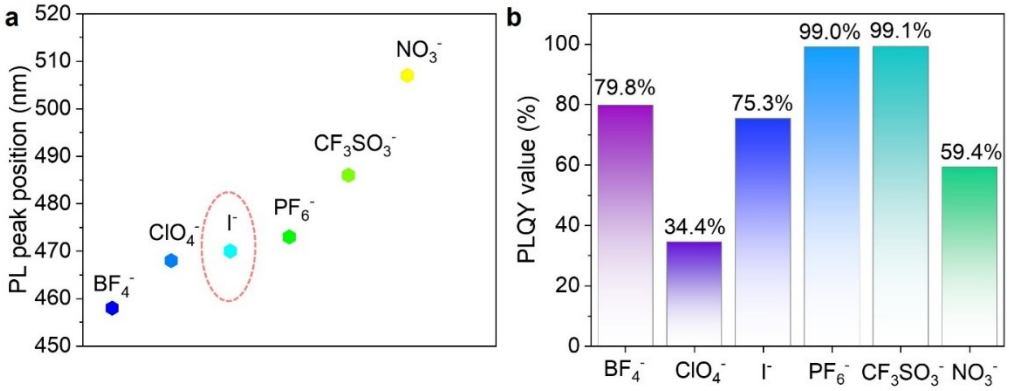

Fig. S6. (a) PL peak positions and (b) PLQY values of C3-X at 300 K.

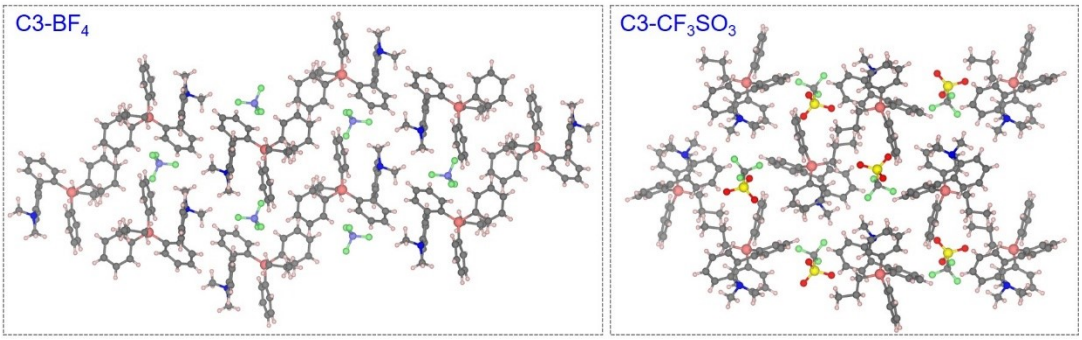

Fig. S7. Crystal structures of C3-BF_4 and C3-CF_3SO_3.

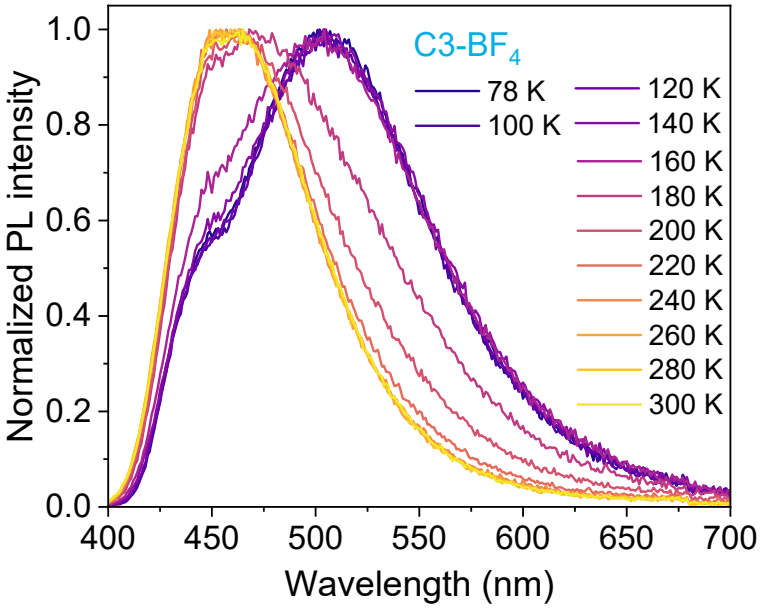

Fig. S8. Temperature-dependent normalized PL spectra of C3-BF_4.

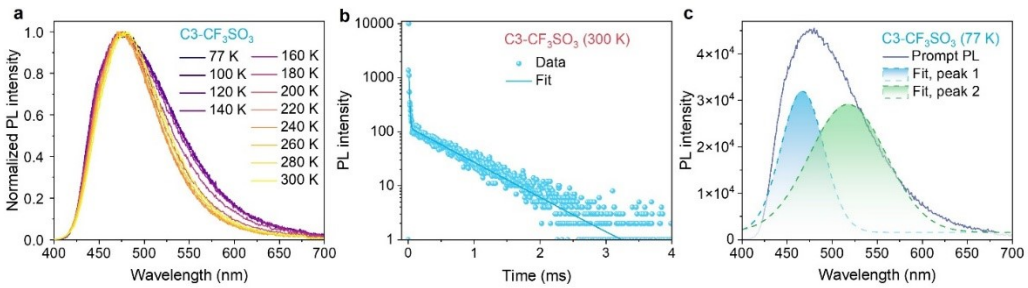

Fig. S9. (a) The TRPL decay curve of C3-CF_3SO_3 at 300 K. (b) Temperature-dependent normalized PL spectra of C3-CF_3SO_3. (c) Fitting result of the prompt PL spectrum at 77 K.

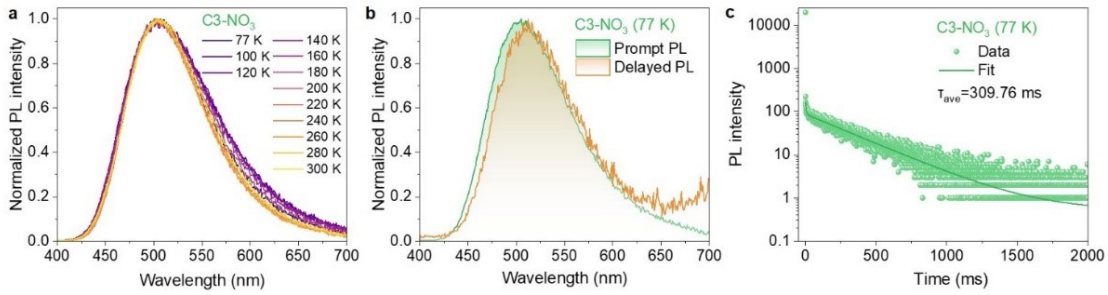

Fig. S10. (a) Temperature-dependent normalized PL spectra of C3-NO_3. (b) Prompt and delayed PL spectra of C3-NO_3. (c) The TRPL decay curve of C3-NO_3 at 77 K.

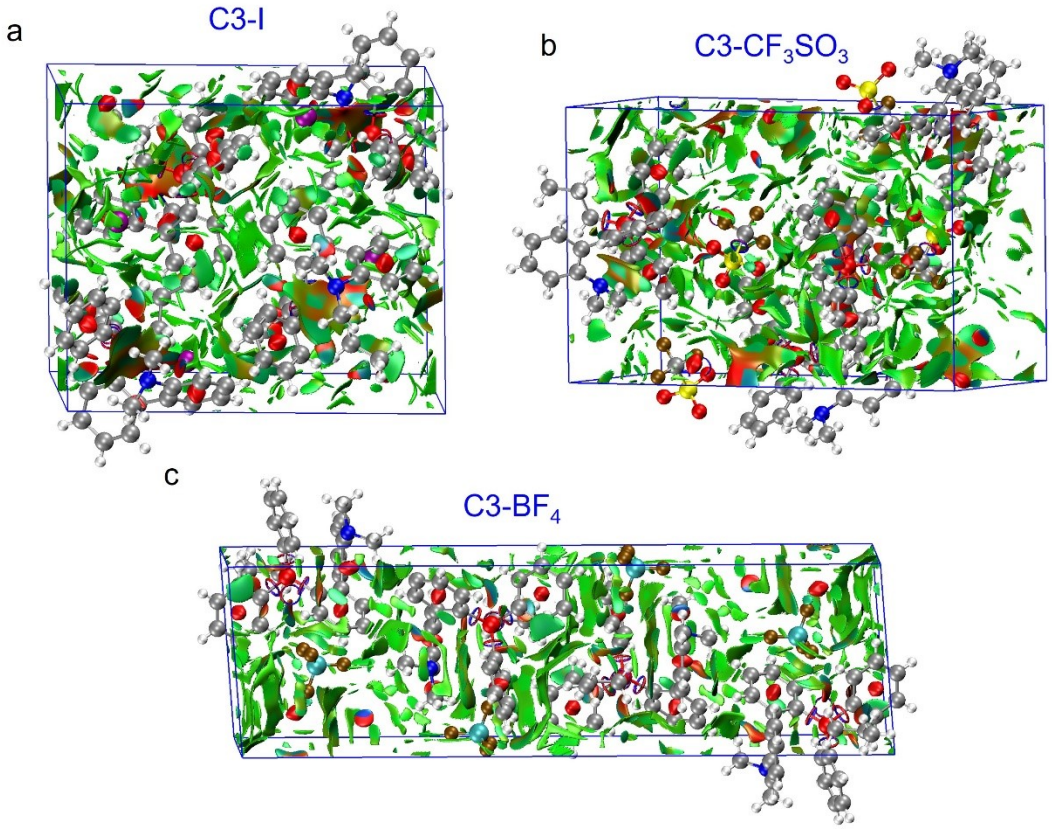

Fig. S11. NCI analyses for (a) C3-I, (b) C3-BF_4, and (c) C3-CF_3SO_3.

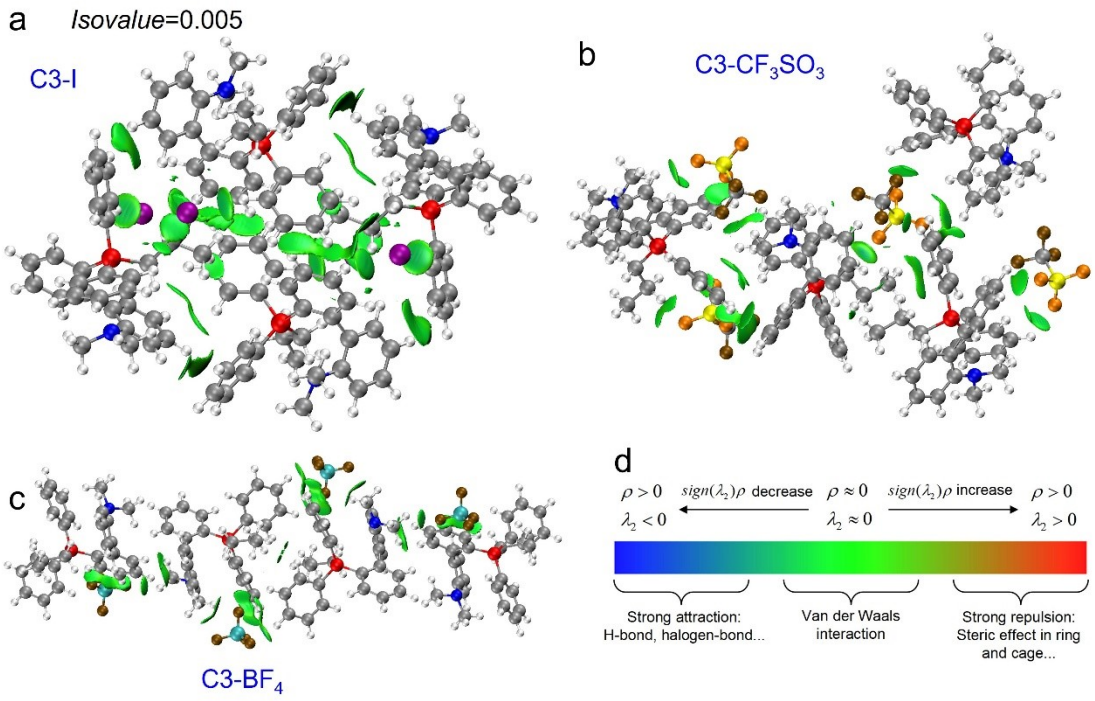

Fig. S12. IGMH analyses for (a) C3-I, (b) C3-BF_4, and (c) C3-CF_3SO_3. (d) Color bar of mapped function $sign(\lambda_2)\rho$ in IGMH maps, the Isovalue is set as 0.005.[11]

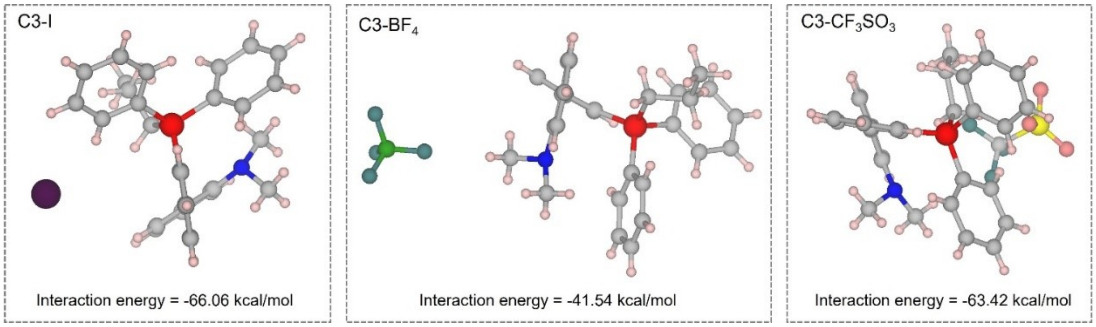

Fig. S13. The asymmetric units and interaction energies of C3-I, C3-BF_4, and C3-CF_3SO_3.

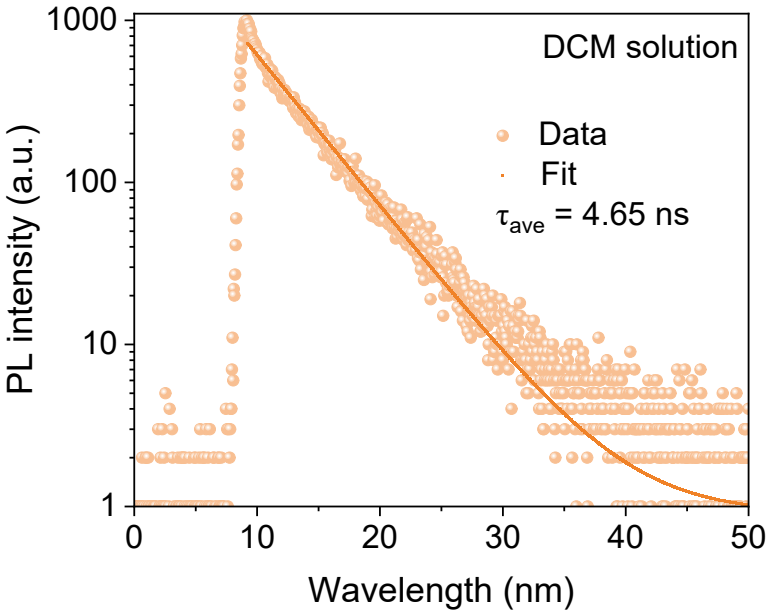

Fig. S14. TRPL decay curve of the C3-I solution in DCM.

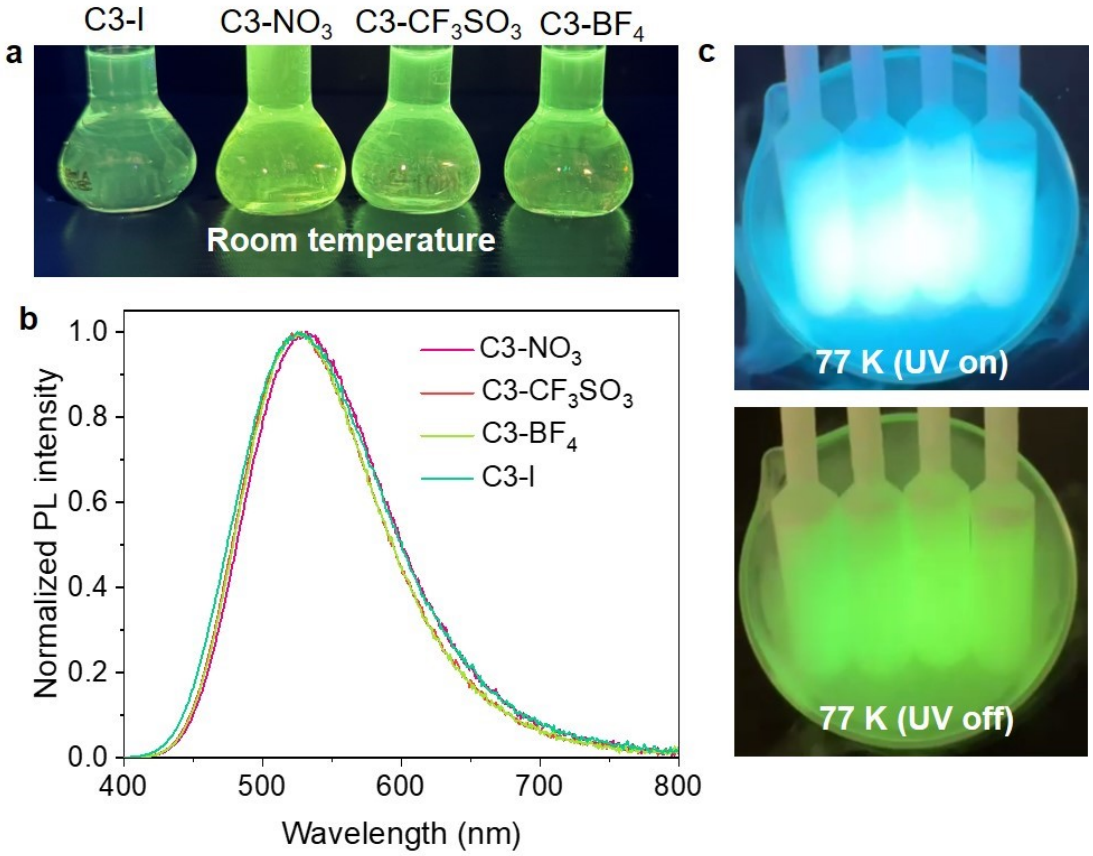

Fig. S15. (a) Photographs and (b) PL spectra of the DCM solutions of C3-I, C3-NO_3, C3-BF_4, and C3-CF_3SO_3 excited at 365 nm. (c) The photographs of the prompt and afterglow emission in DCM solutions of C3-I, C3-NO_3, C3-BF_4, and C3-CF_3SO_3 at 77K.

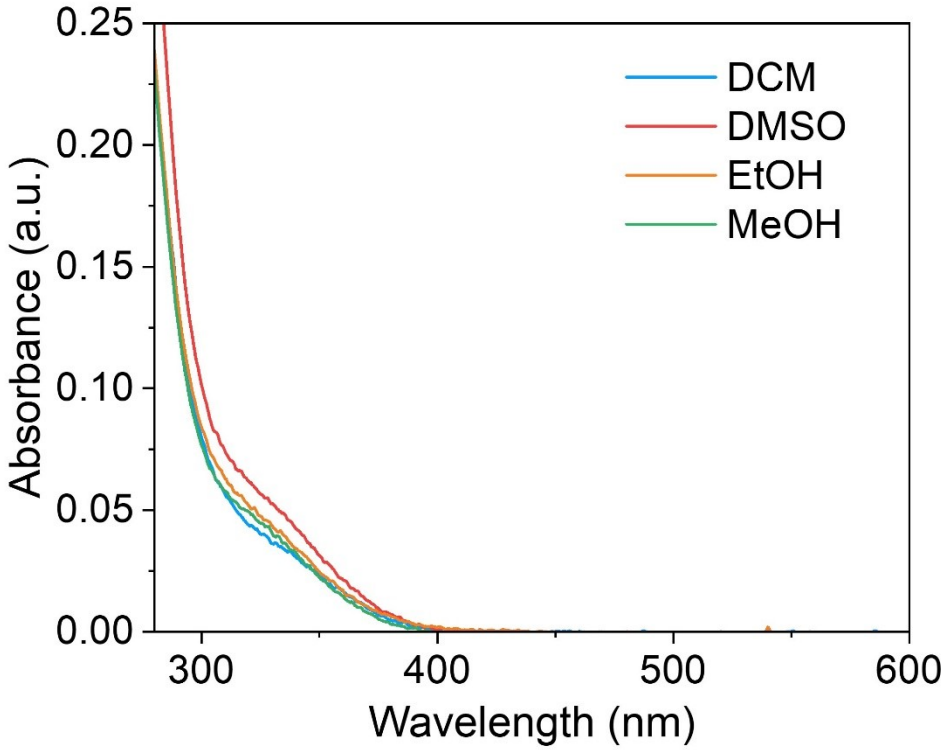

Fig. S16. The absorption spectra of C3-I in the solutions of DCM, DMSO, EtOH, and MeOH.

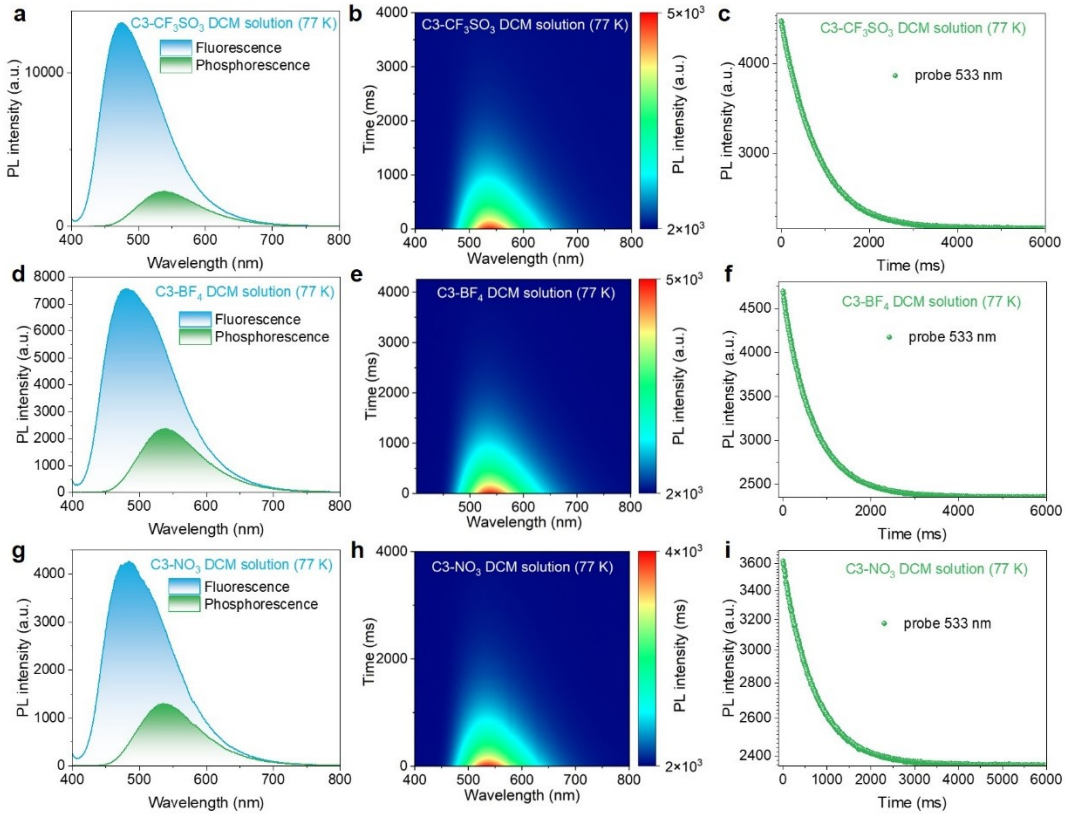

Fig. S17. (a) The prompt and phosphorescence PL spectra, (b) the pseudo-color image of time-resolved PL spectra, and (c) the TRPL decay curve of the C3-CF_3SO_3 DCM solution. (d) The prompt and phosphorescence PL spectra, (e) the pseudo-color image of time-resolved PL spectra, and (f) the TRPL decay curve of the C3-BF_4 DCM solution. (g) The prompt and phosphorescence PL spectra, (h) the pseudo-color image of time-resolved PL spectra, and (i) the TRPL decay curve of the C3-NO_3 DCM solution.

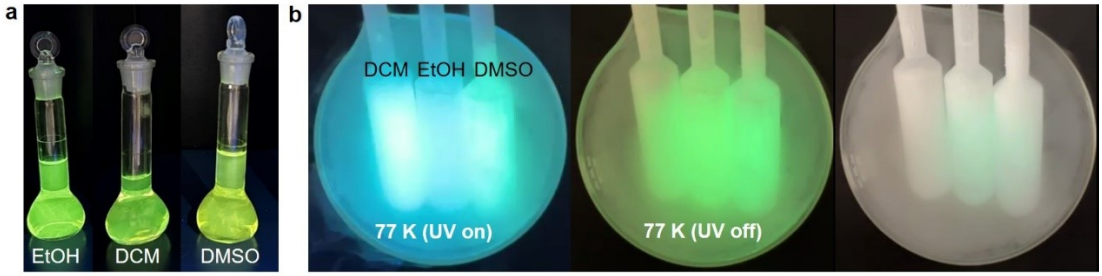

Fig. S18. (a) The photographs of the EtOH, DCM, and DMSO solutions of C3-I. (b) The photographs of the prompt and afterglow emission for the EtOH, DCM, and DMSO solutions of C3-I.

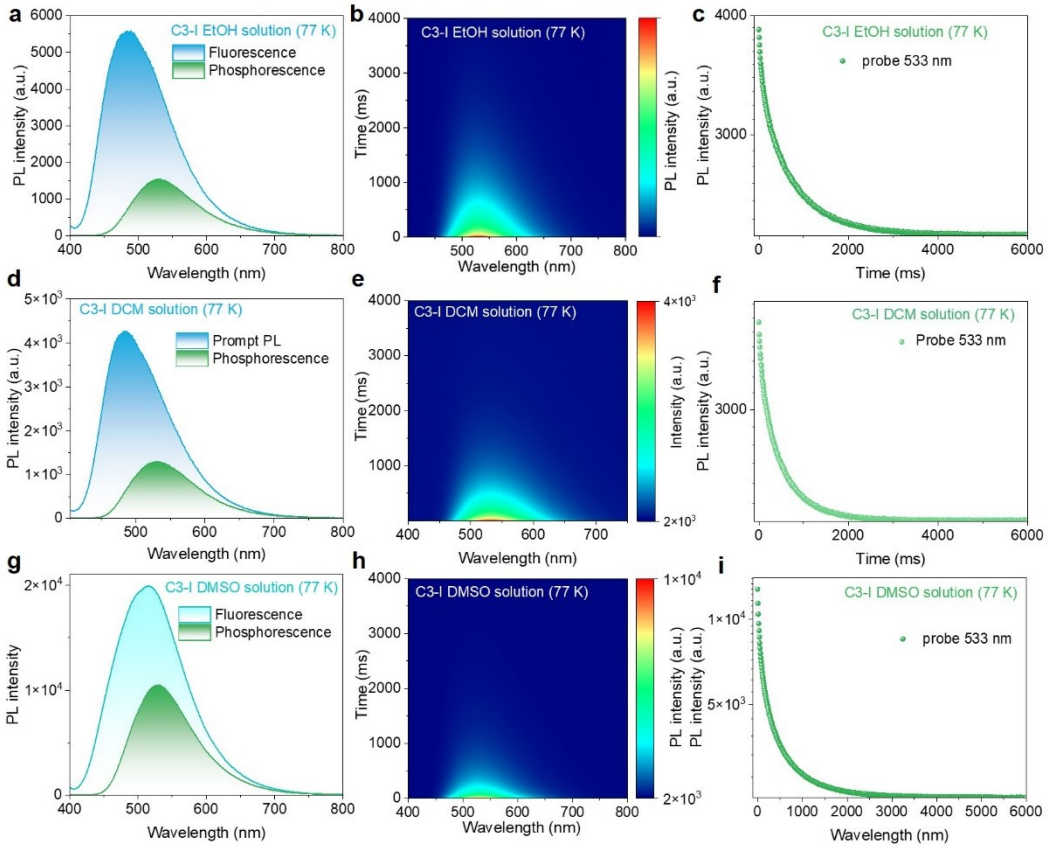

Fig. S19. (a) The prompt and phosphorescence PL spectra, (b) the pseudo-color image of time-resolved PL spectra, and (c) the TRPL decay curve of the C3-I EtOH solution. (d) The prompt and phosphorescence PL spectra, (e) the pseudo-color image of time-resolved PL spectra, and (f) the TRPL decay curve of the C3-I DCM solution. (g) The prompt and phosphorescence PL spectra, (h) the pseudo-color image of time-resolved PL spectra, and (i) the TRPL decay curve of the C3-I DMSO solution.

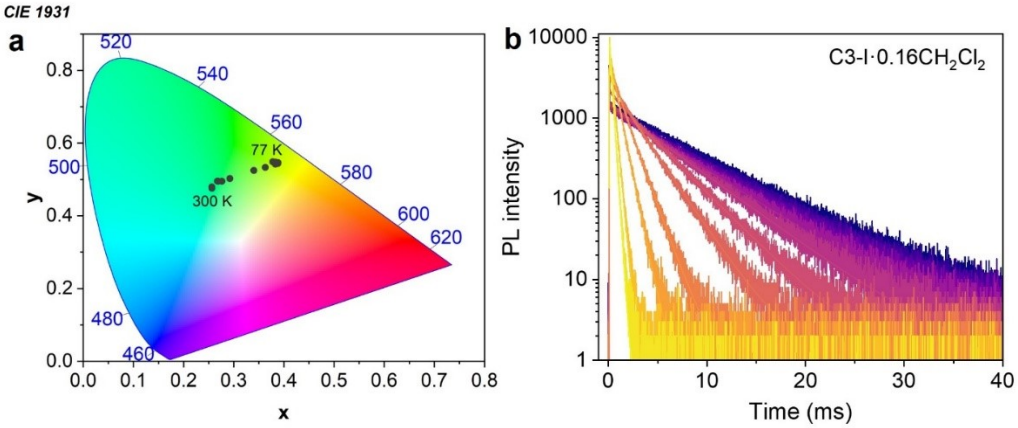

Fig. S20. Temperature-dependent (a) CIE coordinate diagram and (b) TRPL decay curves of C3-I·0.16CH_2Cl_2.

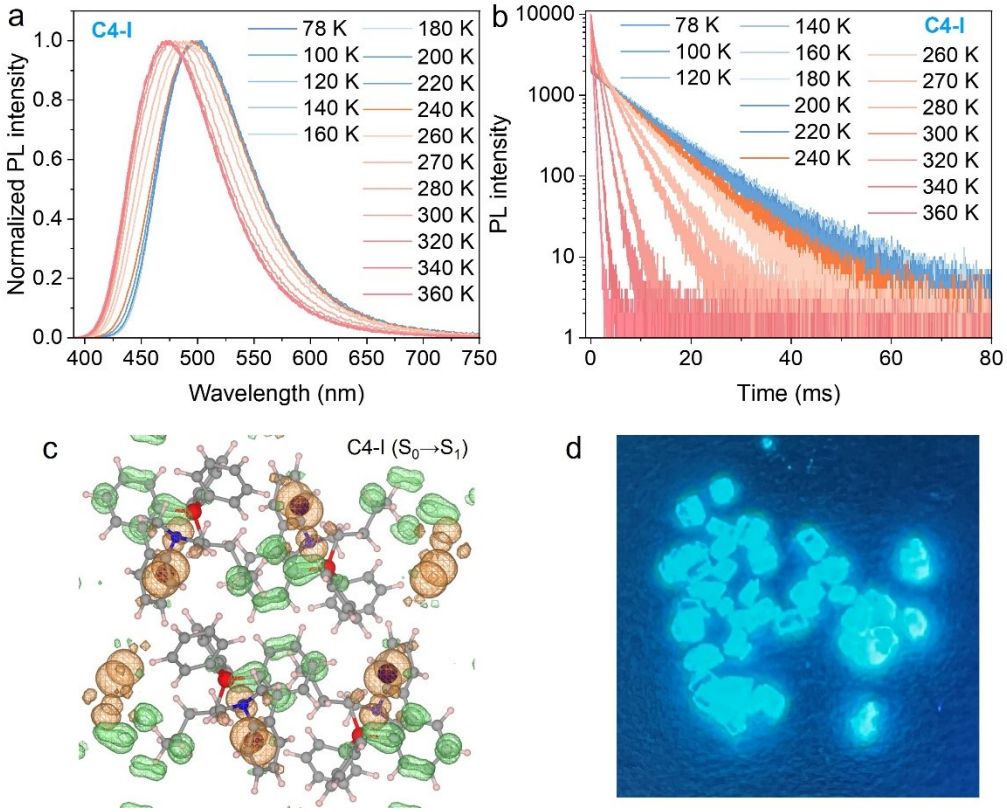

Fig. S21. Photophysical property and electronic transition of C4-I. Temperature-dependent (a) PL and (b) TRPL spectra of C4-I. (c) Charge density difference of $S_0 \rightarrow S_1$ excitation for C4-I. The electron density decreases in the orange area and increases in the green area. (d) The photograph of C4-I single crystals recrystallized from the mixed solvents of ethyl acetate and dichloromethane under UV light.

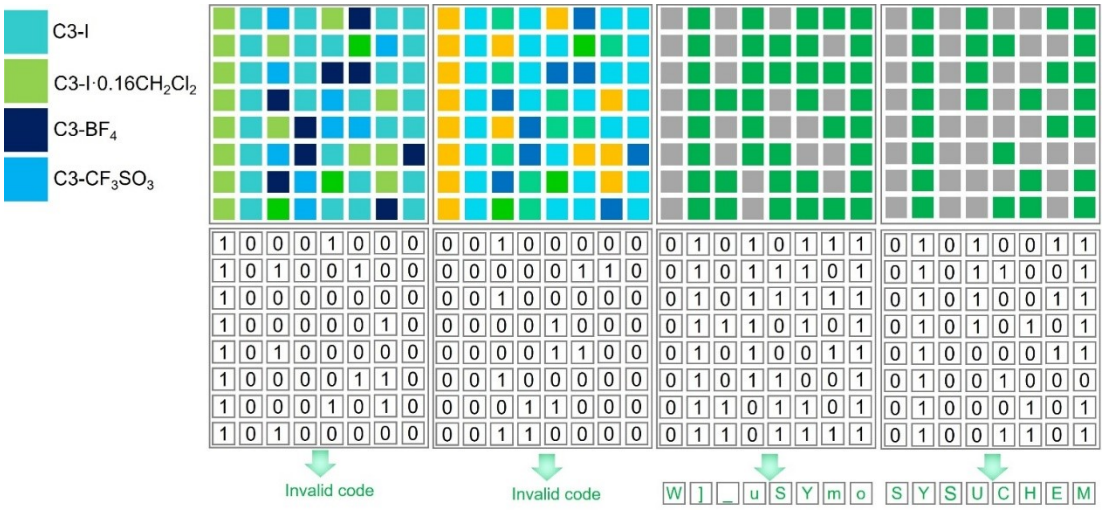

Fig. S22. Graphical illustration of the decryption process.

References

1. J. Hutter, M. Iannuzzi, F. Schiffmann and J. VandeVondele, cp2k: atomistic simulations of condensed matter systems, *WIREs Comput. Mol. Sci.*, 2014, **4**, 15-25.
2. J. P. Perdew, K. Burke and M. Ernzerhof, Generalized Gradient Approximation Made Simple, *Phys. Rev. Lett.*, 1996, **77**, 3865-3868.
3. S. Grimme, Semiempirical GGA-type density functional constructed with a long-range dispersion correction, *J. Comput. Chem.*, 2006, **27**, 1787-1799.
4. S. Goedecker, M. Teter and J. Hutter, Separable dual-space Gaussian pseudopotentials, *Phys. Rev. B*, 1996, **54**, 1703-1710.
5. J. VandeVondele and J. Hutter, Gaussian basis sets for accurate calculations on molecular systems in gas and condensed phases, *J. Chem. Phys.*, 2007, **127**, 114105.
6. A.-S. Hehn, B. Sertcan, F. Belleflamme, S. K. Chulkov, M. B. Watkins and J. Hutter, Excited-State Properties for Extended Systems: Efficient Hybrid Density Functional Methods, *J. Chem. Theory Comput.*, 2022, **18**, 4186-4202.
7. T. Lu and F. Chen, Multiwfn: A multifunctional wavefunction analyzer, *J. Comput. Chem.*, 2012, **33**, 580-592.
8. Z. Liu, T. Lu and Q. Chen, An sp-hybridized all-carboatomic ring, cyclo[18]carbon: Electronic structure, electronic spectrum, and optical nonlinearity, *Carbon*, 2020, **165**, 461-467.
9. K. Momma and F. Izumi, VESTA 3 for three-dimensional visualization of crystal, volumetric and morphology data, *J. Appl. Crystallogr.*, 2011, **44**, 1272-1276.
10. M. J. Frisch, G. W. Trucks, H. B. Schlegel, G. E. Scuseria, M. A. Robb, J. R. Cheeseman, G. Scalmani, V. Barone, G. A. Petersson, H. Nakatsuji, X. Li, M. Caricato, A. V. Marenich, J. Bloino, B. G. Janesko, R. Gomperts, B. Mennucci, H. P. Hratchian, J. V. Ortiz, A. F. Izmaylov, J. L. Sonnenberg, Williams, F. Ding, F. Lipparini, F. Egidi, J. Goings, B. Peng, A. Petrone, T. Henderson, D. Ranasinghe, V. G. Zakrzewski, J. Gao, N. Rega, G. Zheng, W. Liang, M. Hada, M. Ehara, K. Toyota, R. Fukuda, J. Hasegawa, M. Ishida, T. Nakajima, Y. Honda, O. Kitao, H. Nakai, T. Vreven, K. Throssell, J. A. Montgomery Jr., J. E. Peralta, F. Ogliaro, M. J. Bearpark, J. J. Heyd, E. N. Brothers, K. N. Kudin, V. N. Staroverov, T. A. Keith, R. Kobayashi, J. Normand, K. Raghavachari, A. P. Rendell, J. C. Burant, S. S. Iyengar, J. Tomasi, M. Cossi, J. M. Millam, M. Klene, C. Adamo, R. Cammi, J. W. Ochterski, R. L. Martin, K. Morokuma, O. Farkas, J. B. Foresman and D. J. Fox, Gaussian 16 Rev. C.01., 2016.
11. T. Lu and Q. Chen, Interaction Region Indicator: A Simple Real Space Function Clearly Revealing Both Chemical Bonds and Weak Interactions, *Chemistry–Methods*, 2021, **1**, 231-239.